N89-12921

THERMAL BARRIER COATING LIFE PREDICTION MODEL*

B.H. Pilsner, R.V. Hillery, R.L. McKnight, T.S. Cook, K.S. Kim, and E.C. Duderstadt
General Electric
Aircraft Engine Business Group

INTRODUCTION

The objectives of this program are to determine the predominant modes of degradation of a plasma sprayed thermal barrier coating system, and then to develop and verify life prediction models accounting for these degradation modes. The program is divided into two phases, each consisting of several tasks. The work in Phase I is aimed at identifying the relative importance of the various failure modes, and developing and verifying life prediction model(s) for the predominant mode for a thermal barrier coating system. Two possible predominant failure mechanisms being evaluated are bond coat oxidation and bond coat creep. The work in Phase II will develop design-capable, causal, life prediction models for thermomechanical and thermochemical failure modes, and for the exceptional conditions of foreign object damage and erosion.

Currently, work is continuing in Task II of Phase I aimed at developing a preliminary TBC life prediction model. This model will be created by combining the results of the analytical program, the thermomechanical experiments and the results of the failure mechanism examinations of Task I.

TBC SYSTEMS

The primary TBC system consists of a low pressure plasma-sprayed (LPPS) bond coat layer of Ni-22Cr-10Al-0.3Y, an air plasma sprayed yttria partially stabilized zirconia (ZrO_2-8%Y_2O_3) top coat, on a conventionally cast Rene' 80 substrate alloy (Table 1). This bond coat composition has been demonstrated to possess good oxidation resistance and has a large data base as a TBC bond coat. The ZrO_2-8%Y_2O_3 top coat was chosen since numerous studies have shown that zirconia partially stabilized with 6-8 wt.% Y_2O_3 is the best composition for plasma sprayed TBCs (ref. 1). The Rene' 80 substrate was chosen since a large TBC data base exists for this substrate composition.

Four different TBC systems utilizing four different bond coats have been evaluated in the experiment to evaluate the effect of bond coat creep strength on TBC thermal cycle life (Table 2). These four TBC systems also utilize ZrO_2-8%Y_2O_3 top coats and Rene' 80 substrates. TBC system #1 has the same NiCrAlY bond coat utilized in the primary TBC system. TBC systems #2, #3, and #4 have modified NiCoCrAlY bond coats with alloy additions to increase the bond coat creep strength. An aluminide overcoat was used in each of these systems (1-4) to reduce differences in oxidation resistance for the four bond coats. A comparison of the primary TBC system and its counterpart with an aluminide overcoat is shown in Figure 1.

*Work done under NASA Contract NAS3-23943.

THERMAL CYCLE TESTING

Thermal cycle testing is being performed in an automated Rapid Temperature Furnace (Figure 2). The thermal cycles consist of ten minutes heat up, a 45 minute exposure at 1093°C (2000°F), and 15 minutes forced air cooling (Figure 3). This furnace utilizes a lift which automatically cycles the specimens from the upper furnace exposure zone to the lower cooling compartment where a fan provides forced air cooling. Both air and argon pre-exposures have been used to create changes in both bond coat and top coat prior to these thermal cycle tests.

BOND COAT OXIDATION EXPERIMENTS

In the bond coat oxidation experiments, pre-exposures in air or argon were utilized. The goal of pre-exposures in air was to develop oxide scales prior to thermal cycling, while the goal of the pre-exposures in argon was to allow the other thermally activated phenomena present in the air pre-exposures to occur without developing the oxide scale. The intent was to isolate the effect of bond coat oxidation on thermal cycle life.

As reported previously (ref. 2), the specimens pre-exposed in argon failed before the specimens pre-exposed in air (Figure 4). The detrimental effect of argon was believed to be associated with its effect on the type of oxide that forms on the bond coat surface and an in-house program (ref. 3) was performed to help understand this phenomenon. This study indicated that a possible cause of the shortened life was the diffusion of Cr, Ta, W, and other substrate elements to the bond coat/top coat interface during the argon pre-exposure prior to significant bond coat oxidation. The result was a less protective oxide scale.

To further evaluate this phenomenon, an experiment was run in which all specimens (except one set of baselines) received a 10 hour air pre-exposure at 1093°C (2000°F) prior to either air or argon pre-exposures, and thermal cycle testing. In this case, it can be assumed that all specimens developed the same (Al_2O_3) film in the initial air exposure and that the effect of further oxidation of the bond coat would be seen only in those specimens exposed for additional times in air. The results (Figure 5) clearly indicate that continued exposure to air is more detrimental than a prolonged argon exposure (when both are preceded by the air pre-exposure). The larger decrease in thermal cycle life for air exposures is attributed to the continued growth of oxide scales, whereas little or no additional growth occurred in the argon exposures. These results demonstrate the importance of bond coat oxidation to the overall TBC failure mechanism.

Further evidence of the importance of bond coat oxidation is shown by the following observations. Continuous oxide scales of approximately 4 μm were typically observed at the bond coat/top coat interface for the "as-sprayed" and "air pre-exposed" specimens at failure after thermal cycle testing (Figure 6). This observation of a "critical" oxide thickness being necessary to cause failure is consistent with the work of Miller (ref. 4), who noted similar weight changes (oxidation) at failure of specimens with a $CaSiO_4$/MCrAlY TBC, regardless of test temperature.

BOND COAT CREEP EXPERIMENTS

The effect of bond coat creep strength on thermal cycle life was evaluated utilizing four different bond coat alloys (Table II) that had significantly different creep strengths. The modified NiCoCrAlY bond coats include various additions of Mo, Ta, W, Re, Hf, C, B, Si, Zr, and Ti and also received an aluminide (Codep) coating (Figure 1b) as described earlier. All specimens were coated with the same ZrO_2-8%Y_2O_3 ceramic layer. Six specimens of each TBC system were thermal cycle tested. Two were exposed in argon for 100 hours at 1093°C (2000°F), two were exposed in air for the same time and temperature, and two specimens received no pre-exposure. The difference in thermal cycle lives was expected to be a function of bond coat creep strength and pretest conditions.

The results clearly showed that the TBC specimens with the NiCrAlY + aluminide bond coat, which has the lowest creep strength, resulted in the shortest thermal cycle life for all pre-exposure conditions (Figures 7 & 8). However, the thermal cycle life differences for the other TBC systems appears to be minimal. The small differences may indicate that the bond coat creep strength differences (Table II) were not large enough to offset the effect of other failure mechanisms (NiCrAlY is significantly lower in strength than the other three). Interestingly, the 100 hour air pre-exposure did not significantly affect the thermal cycle life of the systems with "high strength" bond coats (Systems 2, 3, and 4). This indicates that, as the thermal cycle life increases (as a result of increasing the bond coat creep strength), the relative contribution of the pre-exposure (oxidation) to the overall failure mechanism is reduced.

In a recent additional study at GE, different bond coat creep strengths were produced by applying various heat treatments to the same bond coat (System #4) to eliminate any differences that might have resulted from aluminide effects on the four bond coats. The results of this study (ref. 5) indicate that TBC thermal cycle life increases with heat treatment temperature (increasing creep strength), again demonstrating that creep strength of the bond coat does indeed influence TBC life.

KEY PROPERTY DETERMINATIONS

Tensile strength, Poisson's ratio, dynamic elastic modulus, and coefficient of thermal expansion for the bond coat were determined from room temperature to approximately 1093°C (2000°F). Standard testing procedures and test specimens were utilized for the NiCrAlY bond coat specimens. The specimens were machined from 5.1 cm (2 inches) by 15.2 cm (6 inches) heat treated LPPS NiCrAlY billets of various heights. The as-sprayed billets received a four hour vacuum heat-treatment at 1093°C (2000°F) to increase the machinability of the billets. The 1093°C heat treatment was chosen since this is the soak temperature utilized in thermal cycle testing. The test results are listed in Table III and IV, and Figures 9 and 10.

Dynamic elastic modulus, dynamic shear modulus, Poisson's ratio, and coefficient of thermal expansion for the top coat were determined from room temperature to approximately 1093°C. In all tests, free-standing air plasma sprayed specimens were utilized and were produced by depositing the ceramic material on stainless steel substrates and inducing a thermal shock to cause spallation of the intact ceramic sheet. Some final machining was required to achieve the desired specimen configurations. These specimens also received a four hour heat treatment in air at 1093°C (2000°F) prior to testing. The test results are listed in Table V and VI,

and Figure 11. Interestingly, the average elastic modulus value determined at room temperature from the bend test (Table V) is a factor of 10 less than the values measured by the resonant frequency method (Table VI). The difference is possibly associated with the presence of cracks, porosity, and splats which would tend to decrease the apparent modulus in the bend test. These factors should play a smaller role in the resonant frequency method.

TBC ANALYTICAL MODELING PROGRAM

Five different analytical tasks, each dealing with a particular aspect of TBC failure, are being investigated using finite element analysis. The first three tasks involve an axisymmetric model (Figures 12 & 13) of a multilayer cylinder, the fourth task examines a disk model, and the fifth task is intended to combine finite element models with simple crack and diffusion models. The specific conditions of each task are discussed below.

Task a. In this evaluation, the same temperature was assumed at the inner and outer surfaces of the specimen (i.e. no gradient across the TBC coated tubular specimen). The GE cyclic temperature rig's cycle (10-minute heat up, 45-minute exposure at 1093°C, 15-minute cooling, Figure 3) was modeled.

Task b. In this task, a temperature distribution generated by a gradient across the TBC cooled tubular specimen is modeled. The work models the effect of the large gradients (100-150°C) developed across the ceramic.

Task c. In this evaluation, cracks will be "placed" along the bond coat/top coat interface, thereby producing a ring crack. One or more cracks perpendicular to the free surface will then be added. The goal is to examine crack tip driving forces to determine any changes resulting from accommodation of displacements by the multiple cracks. Small submodels involving a number of cracks may be studied applying perturbation approaches (localized crack changes). The conditions for this modeling will be based on the results of the first two tasks described above.

Task d. The importance of edge effects in multilayer disk specimens will be evaluated. Since most TBC applications involve edge effects (coating "patches", component edges, cooling holes, etc.), it is important to examine how these edges affect thermal cycle life.

Task e. In this task, the finite element model results from the four preceding tasks, along with some simple elastic crack models, thermal mismatch strains, a diffusion model (e.g., $\ell \propto Dt$), and the effect of hydrostatic pressure to further examine crack tip driving force. Since this is an elastic model only, there are limits on its potential but it is hoped that some significant insight on cracking in ceramics can be gained in this Task.

In the first four tasks of the modeling work, emphasis will be placed on extracting stress and displacement data as a function of time and location under changes in geometry and boundary conditions. In cases where sufficient material

data is available (crack initiation, propagation, or failure data), quantities predicted by the models will be compared to this data for failure information.

The axisymmetric finite element program (Figures 12 & 13) has been applied to the first two analytical tasks. The bond coat stress free temperature was assumed to be 982°C (1800°F), while the top coat stress free temperature was assumed to be 204°C (400°F). These are the temperatures of the substrate during application of these coatings. In the analysis, both elastic and plastic deformation were included, but no plasticity developed for the temperature conditions selected (time at temperature was not included). Analysis of the results for the first two analytical tasks is discussed below.

In Task a, the specimen was assumed to undergo the thermal cycle of 21°C - 1093°C - 21°C in the cycling rig. Since this is a quasistatic test, the entire specimen was assumed to be at a given temperature. Effective, radial, axial, and hoop stresses versus distance in the radial direction are plotted in Figure 14 for four different temperatures [21°C (70°F), 204°C (400°F), 982°C (1800°F), and 1093°C (2000°F)]. As indicated, the stress free temperature for the top coat is 204°C (400°F), therefore, zero stress is found in the top coat at this temperature. However, since the top coat was applied to the bond coat, 982°C (1800°F) is no longer the bond coat stress free temperature. Therefore, small stresses due to the top coat application develop in the bond coat at this temperature.

In the Task b, a temperature distribution across the TBC system was modeled. In this examination, the surface of the ceramic was set at 1093°C (2000°F), the bond coat/top coat interface at 943°C (1730°F), the bond coat/substrate interface at 941°C (1725°F), and the inner wall of the tube at 927°C (1700°F). These results (Figure 15) were plotted and compared with the results present when the system was at 21°C (70°F). Interestingly, the largest effective stress is present in the ceramic near the bond coat/top coat interface which is the typical failure location for thermal barrier coatings. Comparison of the results of deformation behavior for Tasks a and b (Figures 14 and 15) indicate how significantly the presence of thermal gradients can affect the stress state present in TBCs.

THERMOMECHANICAL EXPERIMENTS

Three different thermomechanical experiments have been planned to evaluate the thermomechanical characteristics of TBCs. The primary goal of these examinations is to measure the strains induced during thermal cycling of TBCs, and to relate these strains to the observed failure modes.

In the first experiment, a thermal barrier coated LCF (low cycle fatigue) tube specimen (Figure 16) will be thermally cycled using an induction heating system and a forced air cooling system. The thermomechanical nature of two different thermal cycles will be evaluated. The first thermal cycle will be as close to the GE cyclic temperature rig's cycle (Figure 3) as possible. This experiment is aimed at determining the magnitude of strains induced by thermal cycling of the TBC specimen under essentially zero mechanical load. This experiment will also attempt to determine if any phasing exists between the strains observed for the substrate and the ceramic, or if the ceramic simply follows the displacement of the metal substrate.

In the second experiment, a thermal barrier coated LCF tube specimen will again be thermally cycled using an induction heating system and a forced air cooling system. Tensile, compressive, and zero loading will be applied to three TBC specimens and these specimens will be thermally cycled to failure. The goal is to evaluate the effect of compressive and tensile loading on TBC thermal cycle life.

In the third experiment, the thermal barrier coating will be applied to thin Rene' 80 (substrate) strips which will then be heated and cooled using induction heating and forced air cooling. It is anticipated that the thin Rene' 80 strips and their TBC coatings will bend measurably during thermal transients because of the stresses induced by thermal expansion differences. Values of the curvature changes during coating deposition and during subsequent thermal transients will be compared to predicted curvatures based on natural properties of Rene' 80 and the coating materials. This data, in conjunction with data from the uncoated Rene' 80 strip and free-standing ceramic strip should provided insight into the behavior of coated specimens, and thus contribute to a better understanding of the thermomechanical characteristics of TBCs.

REFERENCES

1. Stecura, S., "Effects of Compositional Changes on the Performance of a Thermal Barrier Coating System," NASA TM 78976, 1979.

2. Hillery, R.V. and Pilsner, B.H., "Thermal Barrier Coating Life Prediction Model - First Annual Report," NASA CR - 175010, 1985.

3. Saegusa, F., "Failure Mechanism Studies on Thermal Barrier Coatings," GE Internal Communication.

4. Miller, R.A., "High Temperature Protective Coatings," S.C. Singhal, Editor, AIME, page 293, 1982.

Table I

BASELINE THERMAL BARRIER COATING SYSTEM (WEIGHT PERCENT)

Substrate (Rene '80): Ni-14Cr-9.5Co-5Ti-4W-4Mo-3Al-0.17C-0.03Zr-0.015B

Bond Coating : Ni-22Cr-10Al-0.3Y (Low Pressure Plasma Spray)

Top Coating : ZrO_2-$8Y_2O_3$ (Air Plasma Spray)

Table II

BOND COAT CREEP EFFECT TBC SYSTEMS

Systems	Substrate	Bond Coating	Over Coating	Top Coating	Bond Coat Creep (Larson/Miller Parameter @ 3 KSI - rupture test)
1	Rene'80	Bond Coating 1'	Aluminide	ZrO_2-Y_2O_3	39.0
2	Rene'80	Bond Coating 2*	Aluminide	ZrO_2-Y_2O_3	45.7
3	Rene'80	Bond Coating 3*	Aluminide	ZrO_2-Y_2O_3	47.0
4	Rene'80	bond Coating 4*	Aluminide	ZrO_2-Y_2O_3	48.4

' Ni-22Cr-10Al-0.3Y

* Modified NiCoCrALY bond coats

Table III

LPPS Ni-22Cr-10Al-0.3Y BOND COAT TENSILE PROPERTIES

TEST TEMPERATURE °C	ULTIMATE STRENGTH MPa	0.2 YIELD MPa	% ELONGATION	% REDUCTION IN AREA
Ambient 25° (77°F)[1]	1320 (191 KSI)	--	--	--
538°C (1000°F)[2]	1240 (179 KSI)	1120 (162 KSI)	5.2	6.2
760°C (1400°F)[2]	450 (65 KSI)	160 (23 KSI)	18.3	19.6
1038°C (1800°F)[3]	16 (2.3 KSI)	13 (1.9 KSI)	149.3	95.6
1093°C (2000°F)[3]	4 (0.6 KSI)	3 (0.4 KSI)	248.3	92.4

[1]No measurable plastic deformation (1 specimen)

[2]Average of three test specimens.

[3]Average of two test specimens.

Table IV

ELASTIC MODULI AND POISSON'S RATIO OF LPPS Ni-22Cr-10Al-0.3Y

Temperature °C	E (Axial) GPa	E (Diametral) GPa	Poisson's Ratio
20 (R.T.)	206 (29.9 MSI)	696 (100.8 MSI)	0.30
538 (1000°F)	180 (26.1 MSI)	602 (87.3 MSI)	0.30
760 (1400°F)	101 (14.7 MSI)	273 (39.6 MSI)	0.37
982 (1800°F)	--	--	--*
1093 (2000°F)	--	--	--*

* No linear portion to stress/strain curves.

Table V

MECHANICAL TESTING OF PLASMA-SPRAYED ZIRCONIA BARS
BEND TEST

Sample I.D.	Width, cm	Thickness, cm	Length, cm	Ultimate Load, Kg (lb)	Ultimate Stress MPa (ksi)	Strain to Failure $in/inx10^{-3}$	Elastic Modulus GPa (MSI)
1-1	0.648	0.238	5.746	7.03 (15.5)	53.3 (7.73)	2.89	19.9 (2.80)
1-2	0.648	0.235	5.747	6.21 (13.69)	56.8 (8.23)	3.07	20.5 (2.92)
1-3	0.648	0.232	5.746	5.26 (11.59)	49.3 (7.15)	2.59	21.8 (3.15)
				Average Elastic Modulus		20.6 GPa (2.98 MSI)	

Table VI

ELEVATED TEMPERATURE DETERMINATION OF ELASTIC MODULUS, SHEAR MODULUS,
AND POISSON'S RATIO OF APS ZrO_2-$8Y_2O_3$

Temp., °C	Resonant Frequency (Hz) Flexural	Torsional	E Elastic Modulus GPa (MSI)	G Shear Modulus GPa (MSI)	Poisson's Ratios
25*	1472	3697	210 (30.5)	91 (13.2)	0.15
25	1466	3672	208 (30.2)	90 (13.1)	0.16
100	1453	3630	205 (29.7)	88 (12.8)	0.16
150	1444	3610	202 (29.3)	87 (12.6)	0.16
200	1436	3573	200 (29.0)	86 (12.4)	0.17
300	1425	3443	197 (28.6)	79 (11.5)	0.24
400	1412	3343	193 (28.0)	75 (10.8)	0.29
450	1411	3325	193 (28.0)	74 (10.7)	0.31
500	1401	3299	190 (27.6)	72 (10.5)	0.31
538	1395	3281	189 (27.4)	72 (10.4)	0.31
600	1387	3265	187 (27.1)	71 (10.3)	0.31
700	1375	3209	184 (26.6)	69 (10.0)	0.33
800	1360	3160	179 (26.0)	67 (9.7)	0.34
900	1342	3135	175 (25.3)	66 (9.5)	0.33
982	1340	3122	175 (25.3)	65 (9.4)	0.34
1000	1362	3147	179 (26.1)	66 (9.6)	0.36
1038	1374	3163	183 (26.5)	67 (9.7)	0.37
1093	1342	3185	175 (25.3)	68 (9.8)	0.29

* Specimen suspended on cotton thread, all others suspended on Pt wire.

"NiCrAlY" Bond Coat TBC

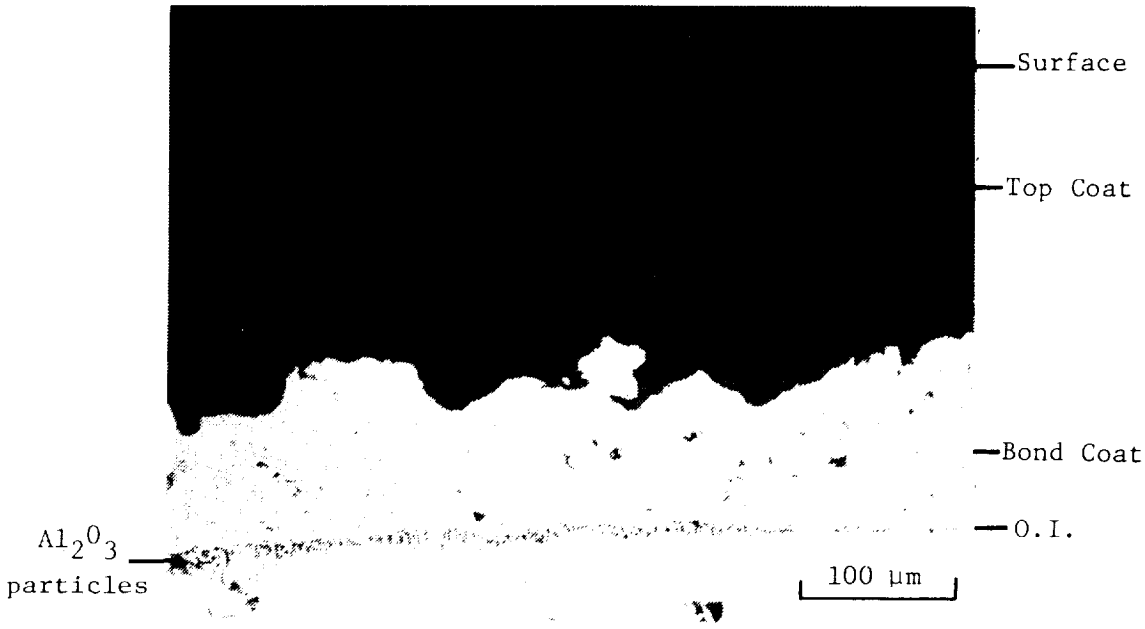

Figure 1a

"NiCrAlY + Codep" Bond Coat TBC

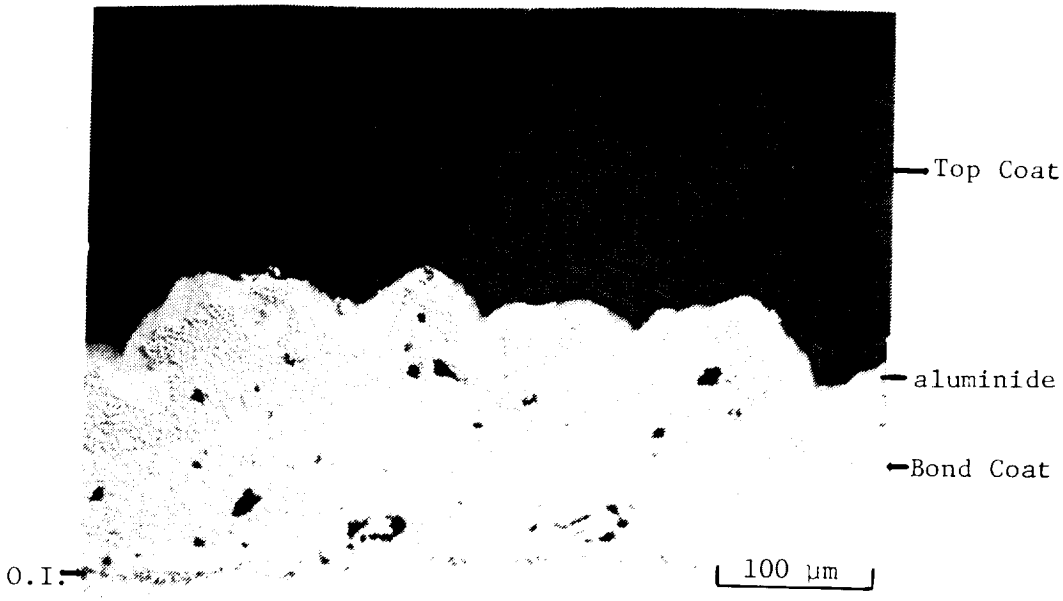

Figure 1b

RAPID TEMP FURNACE

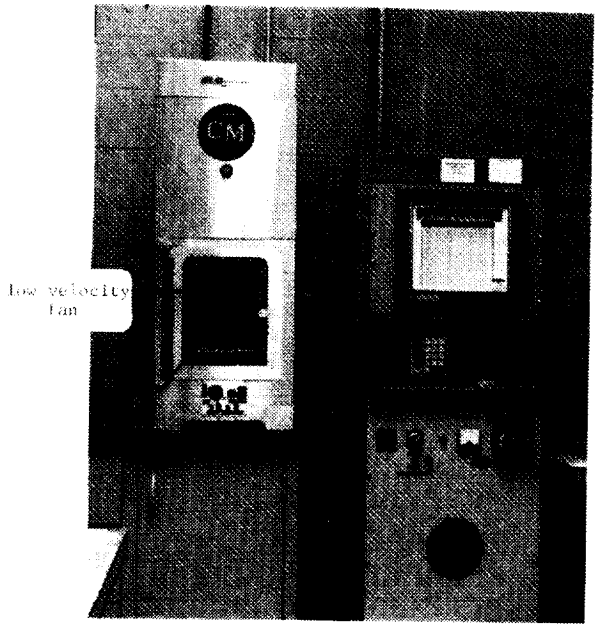

Figure 2

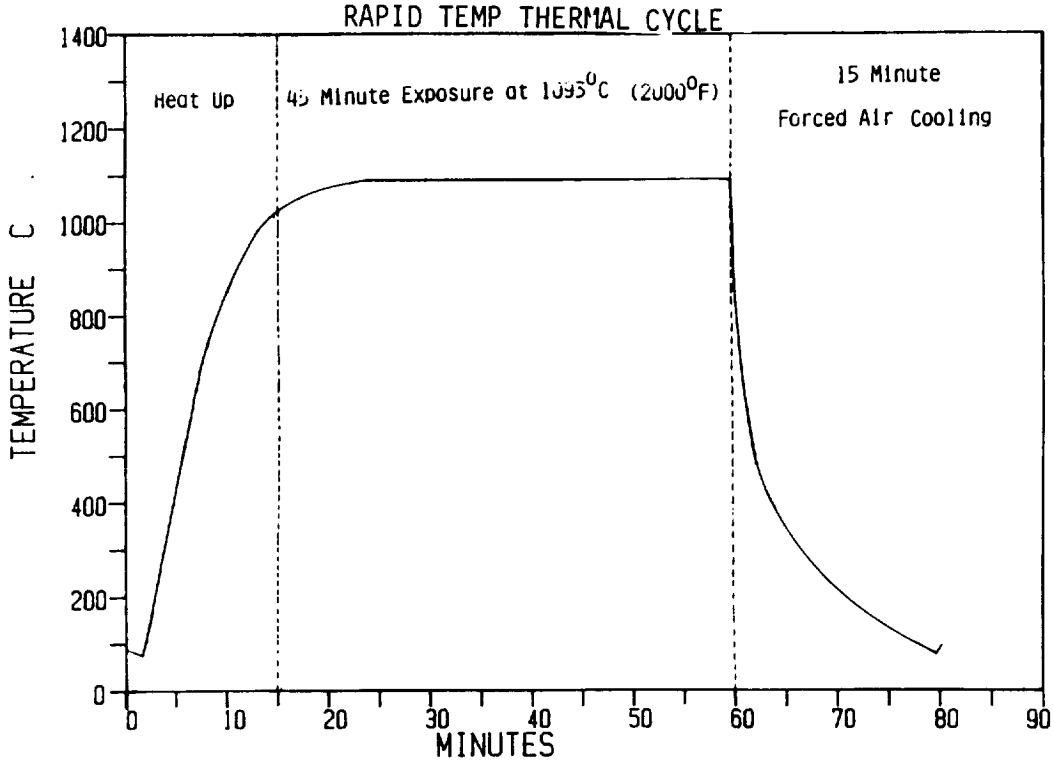

Figure 3

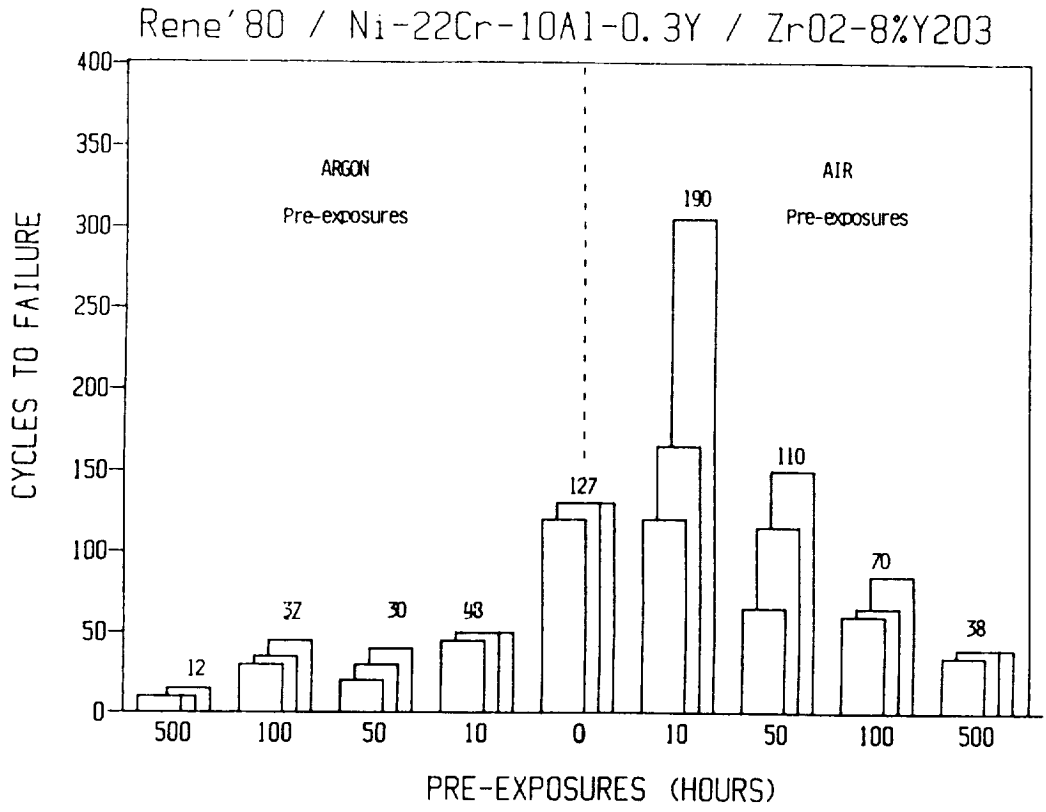

Figure 4

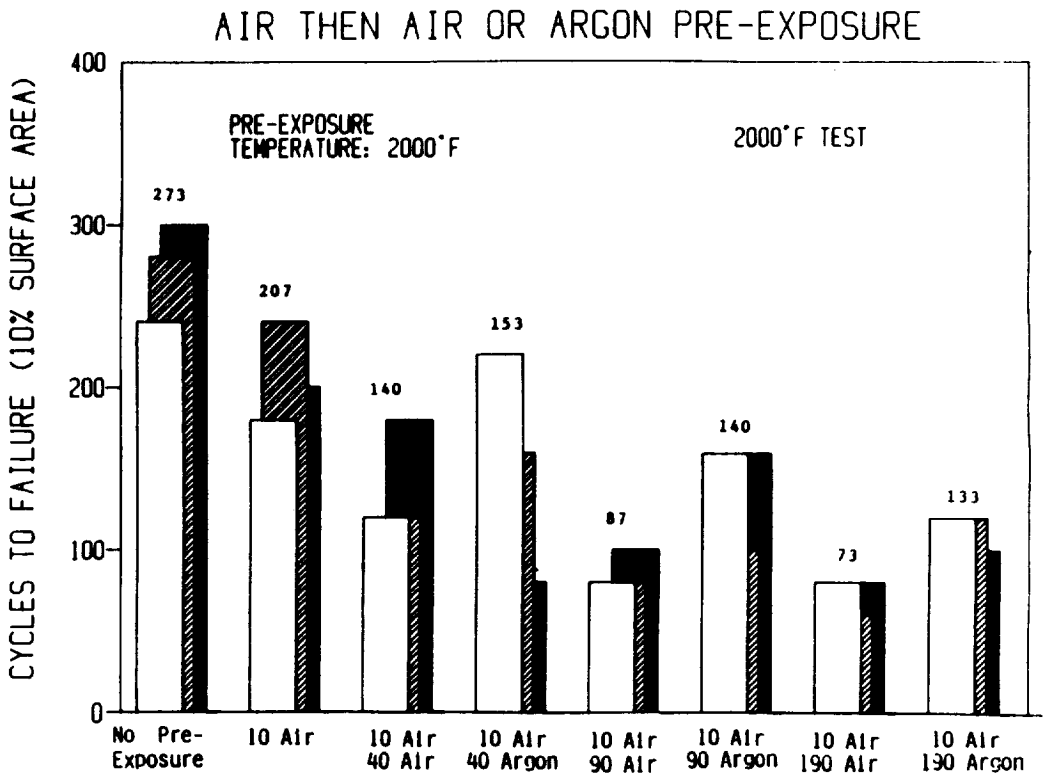

Figure 5

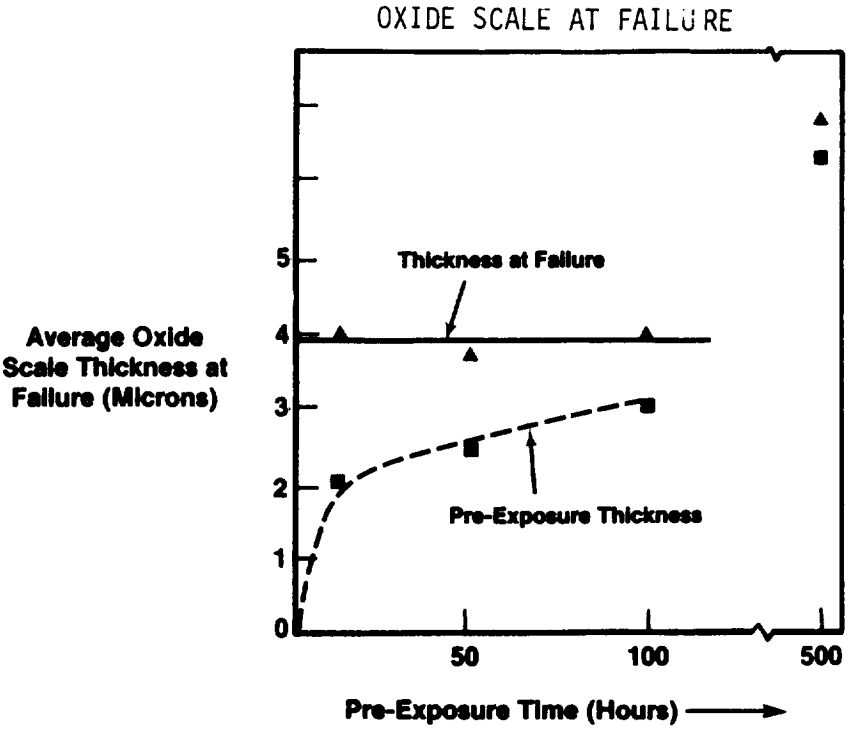

Figure 6

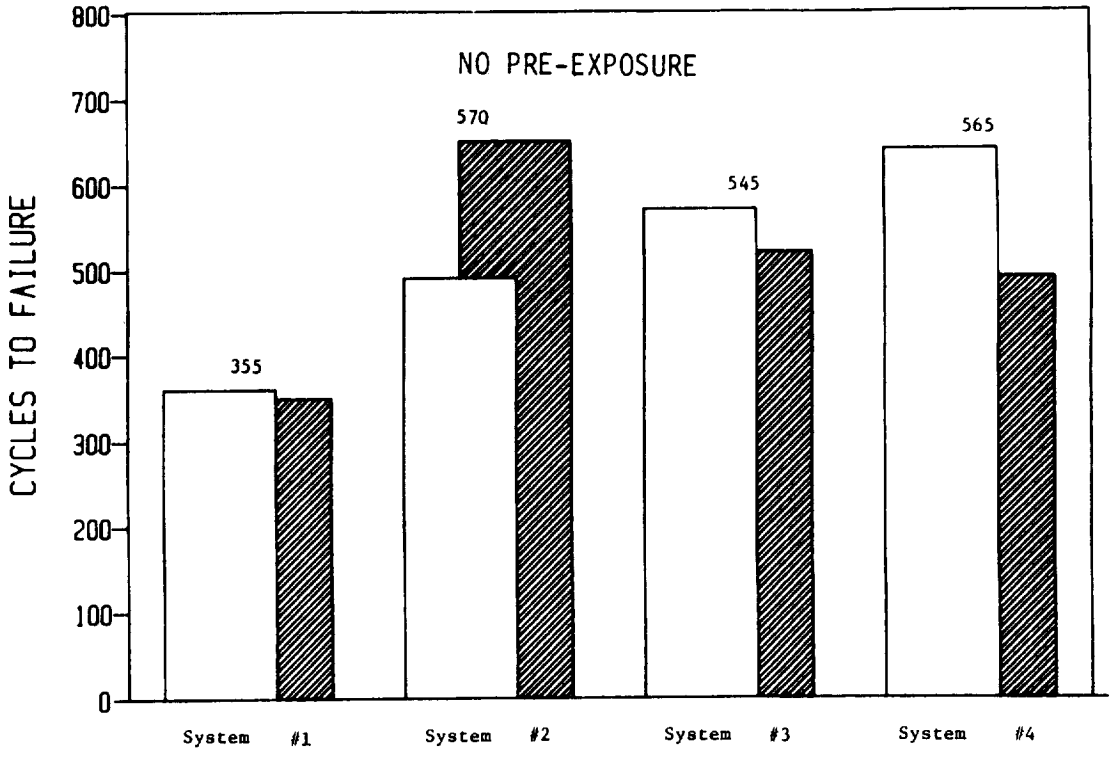

Figure 7

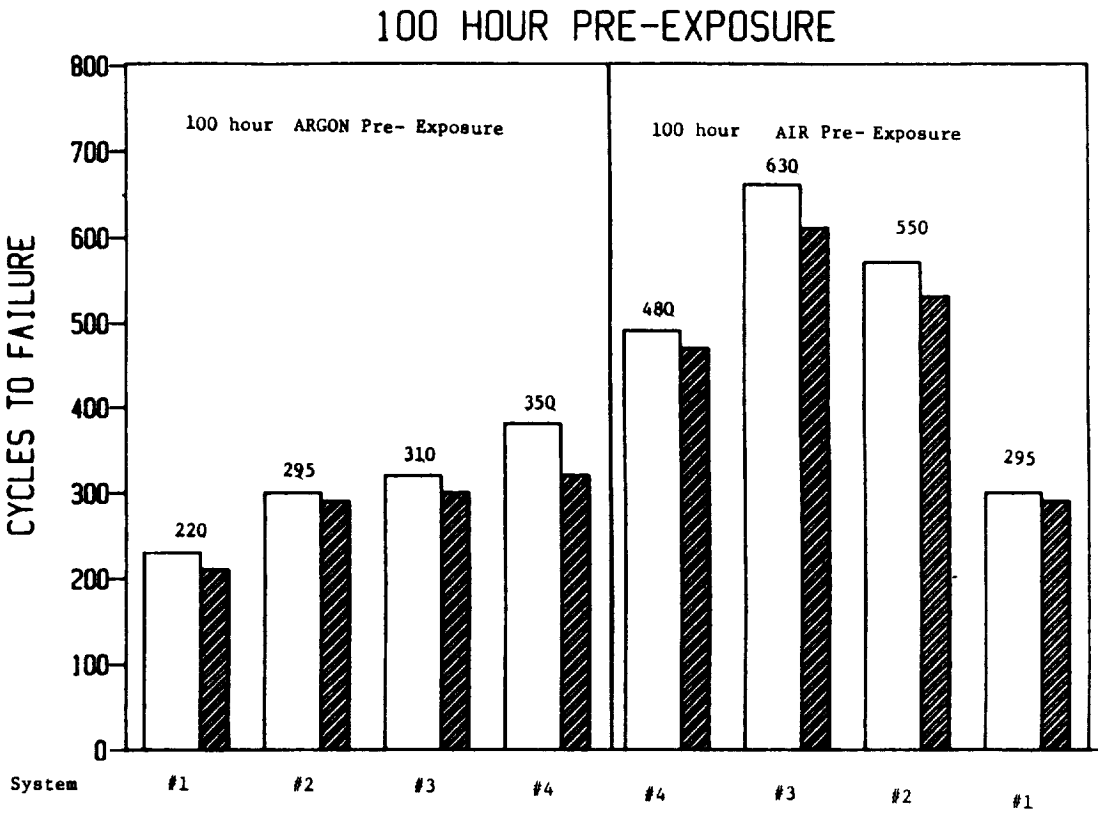

Figure 8

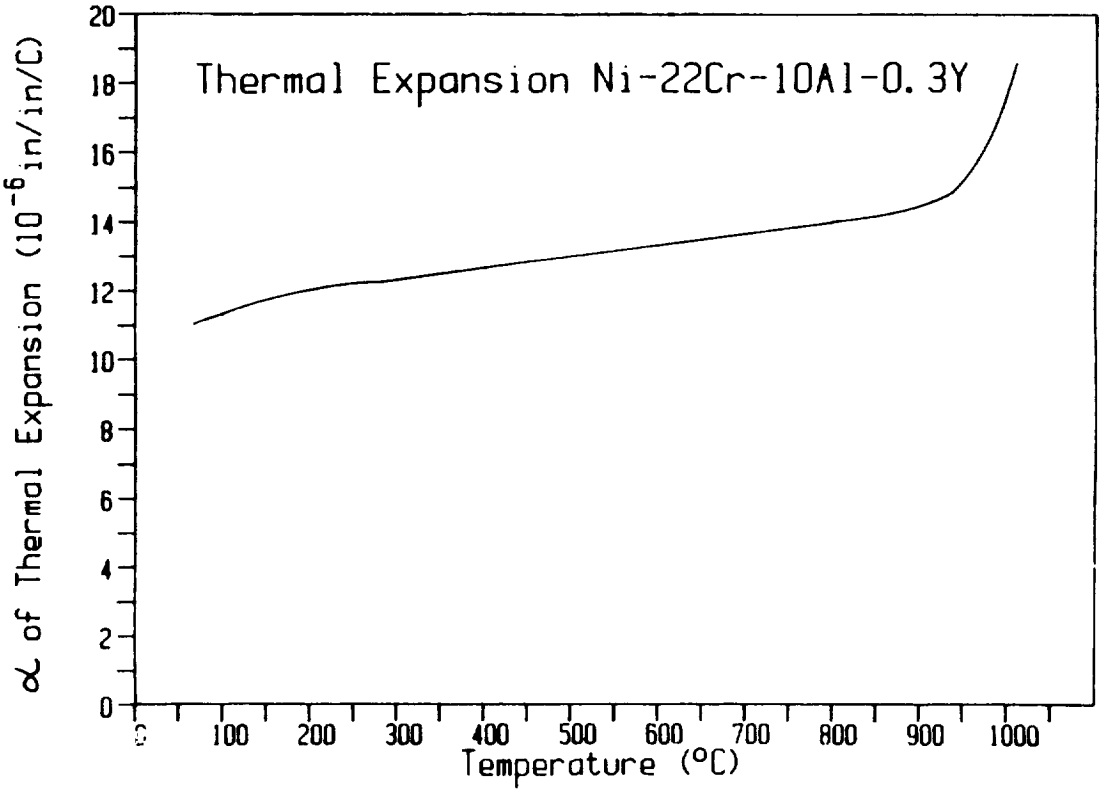

Figure 9

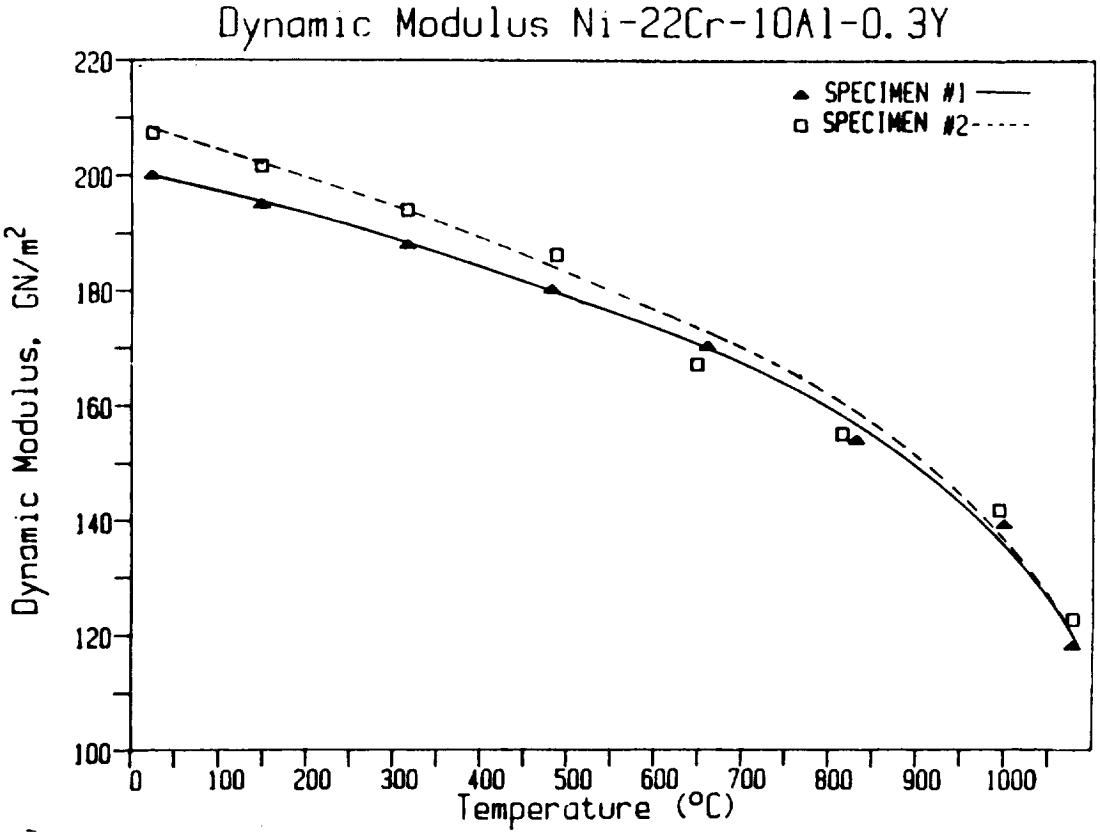

Figure 10

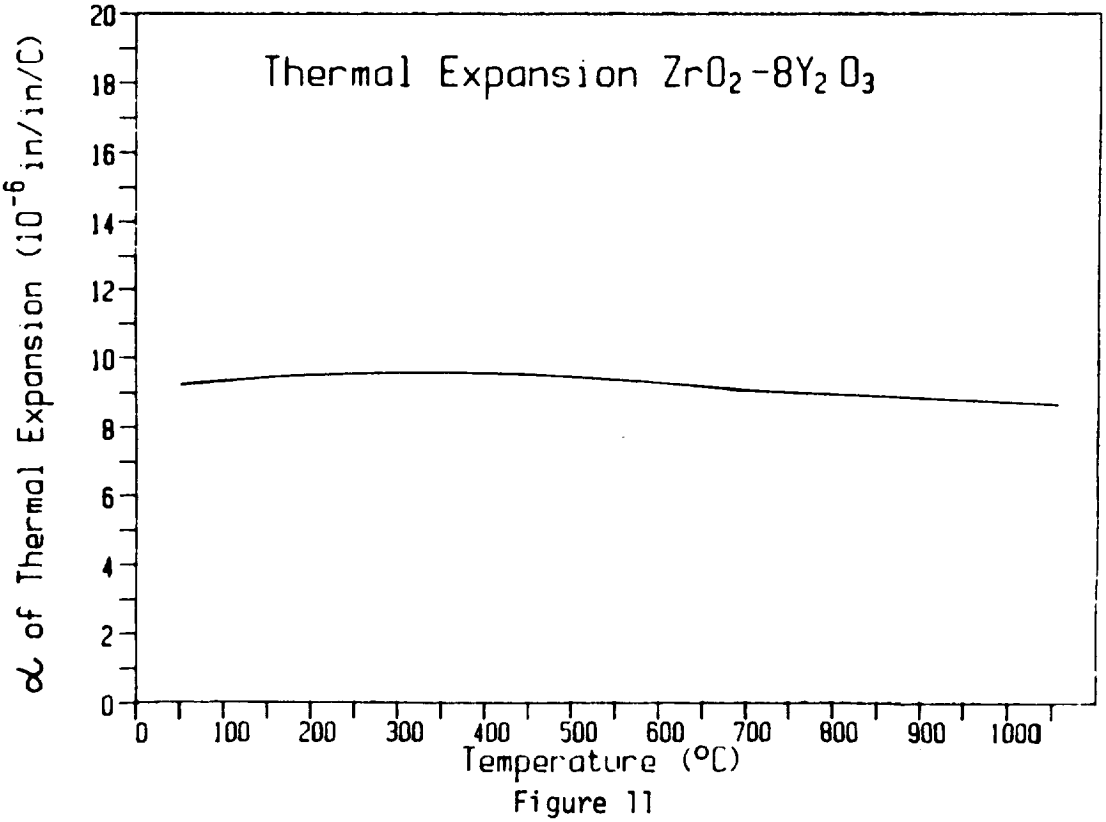

Figure 11

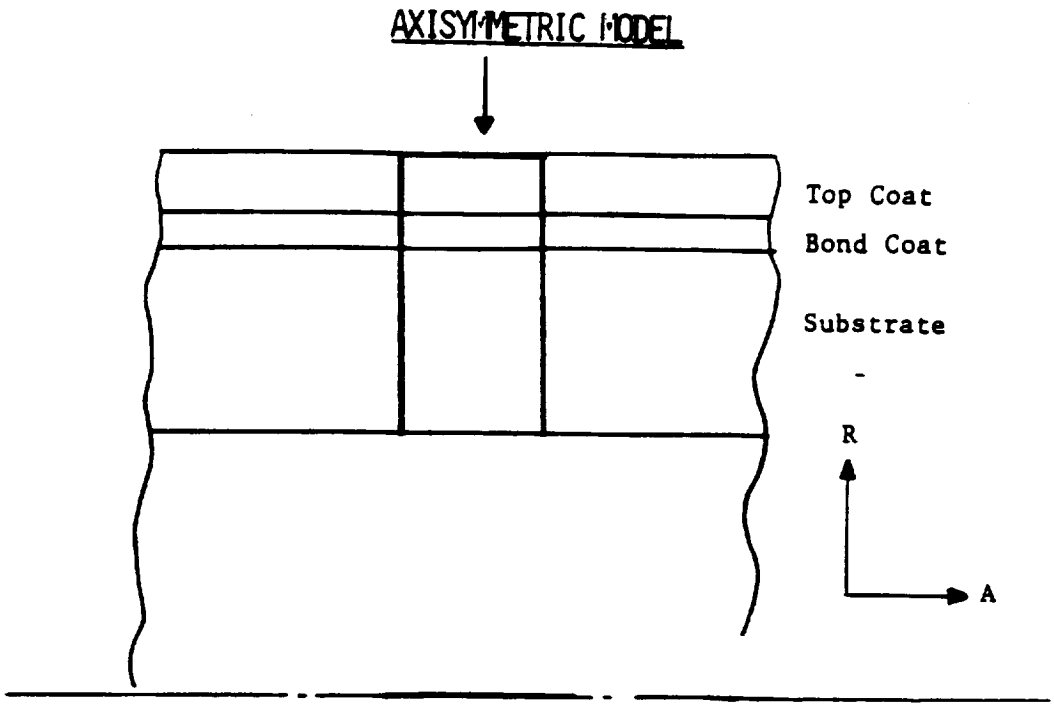

Figure 12

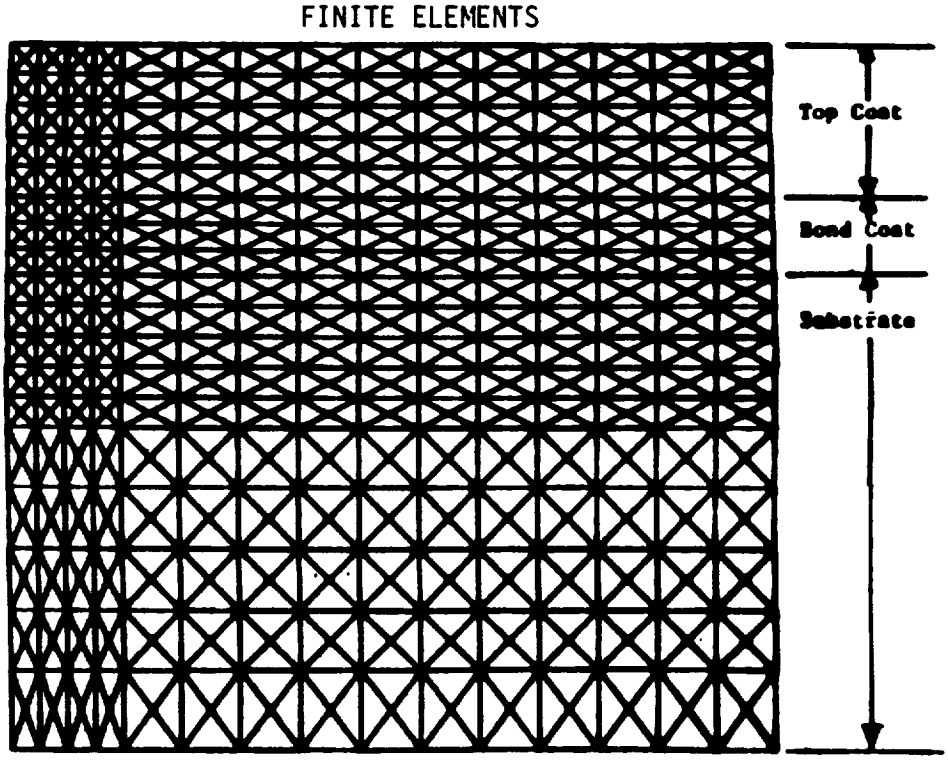

Figure 13

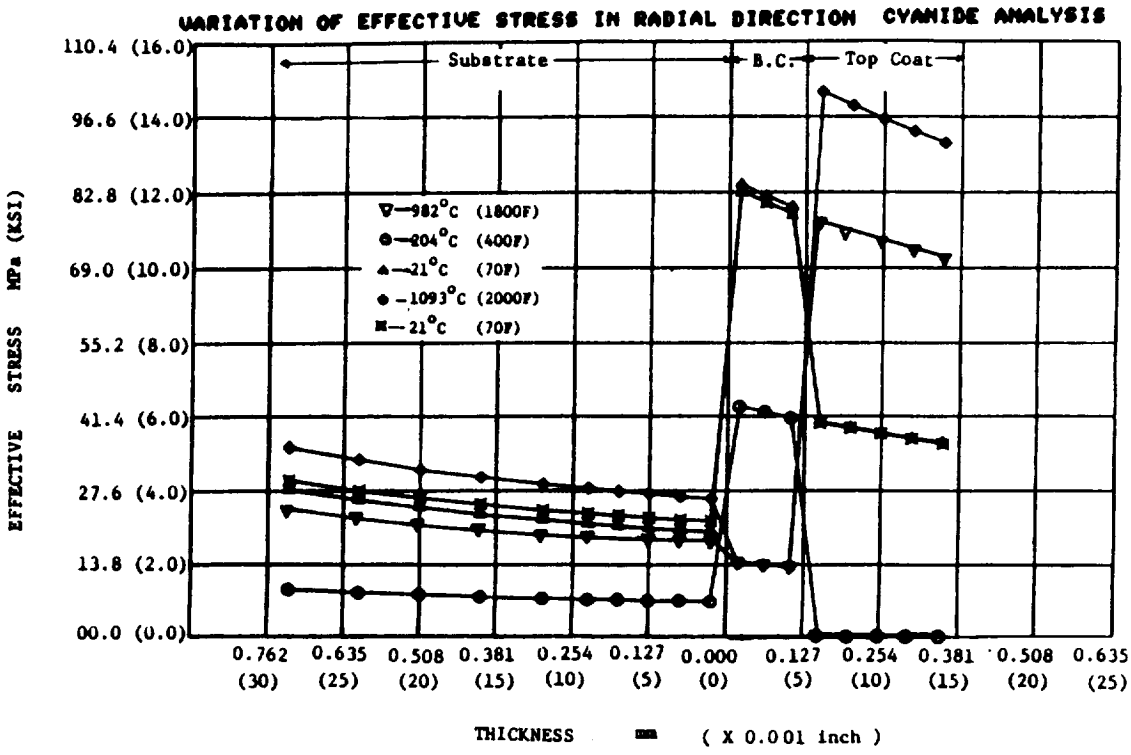

Figure 14a

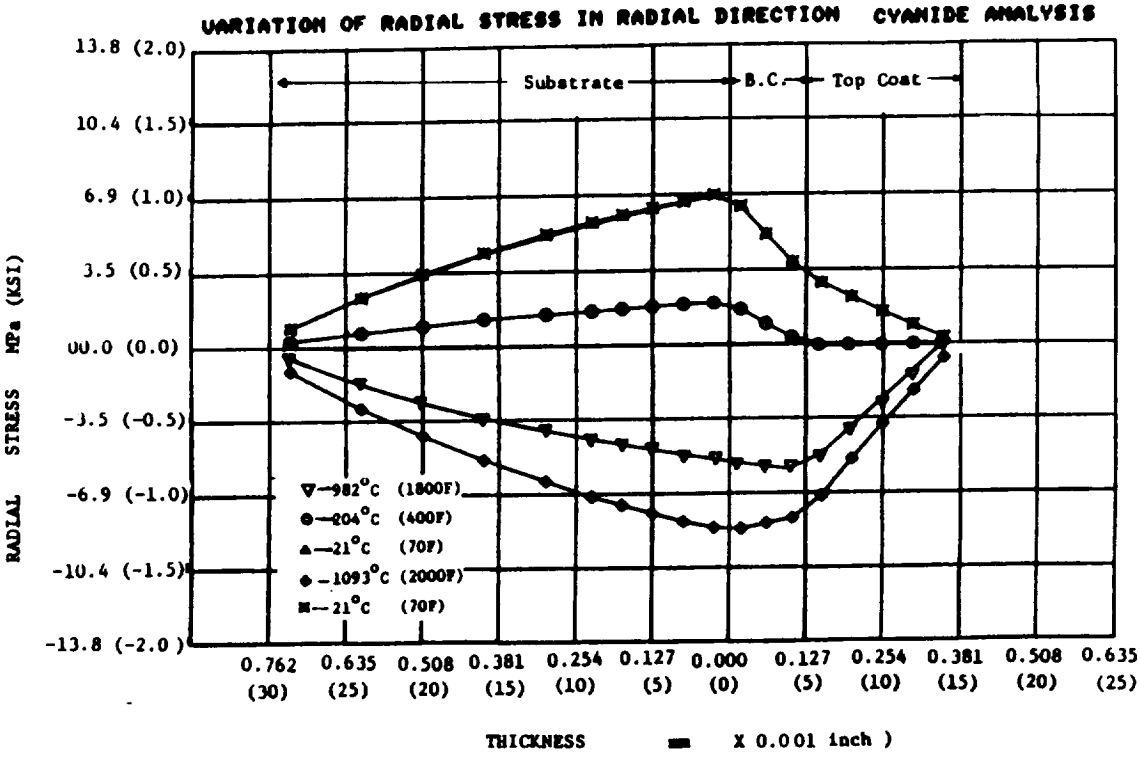

Figure 14b

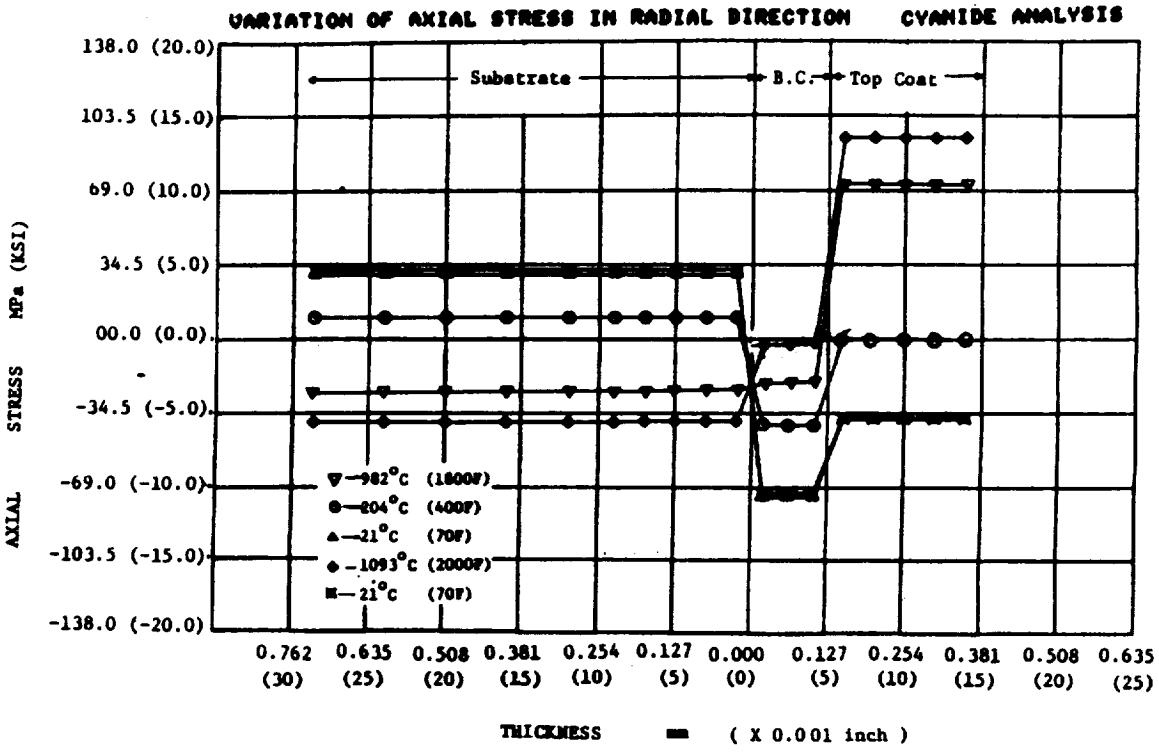

Figure 14c

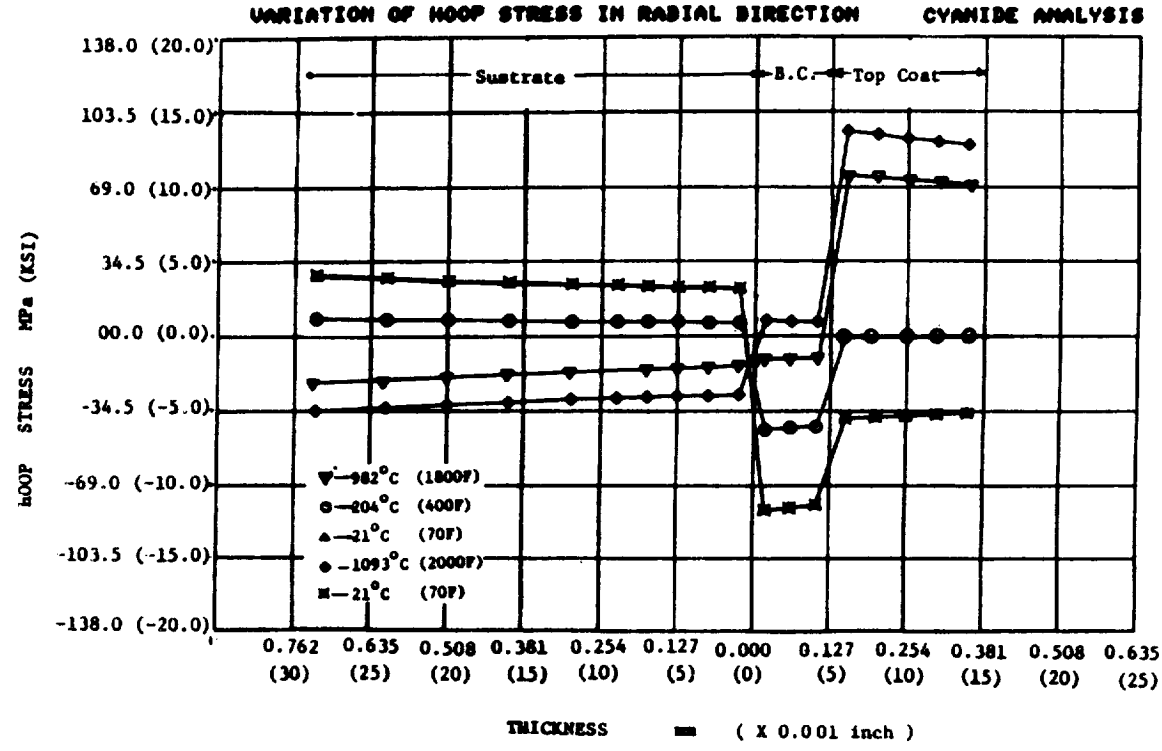

Figure 14d

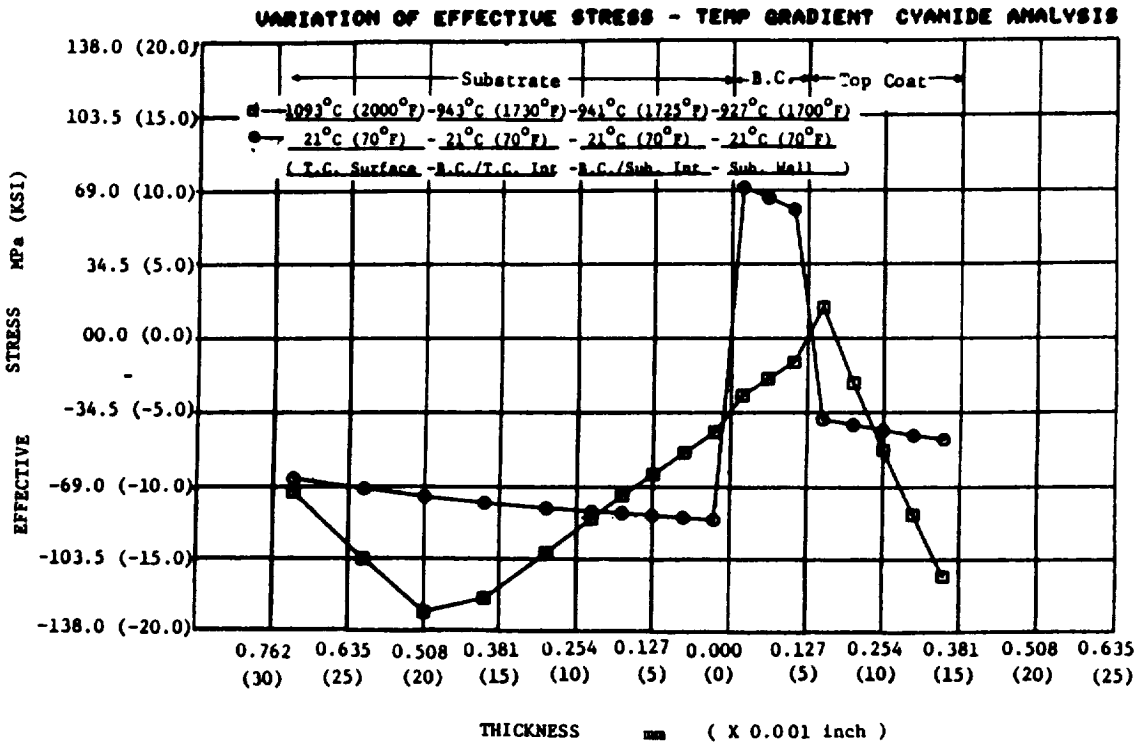

Figure 15a

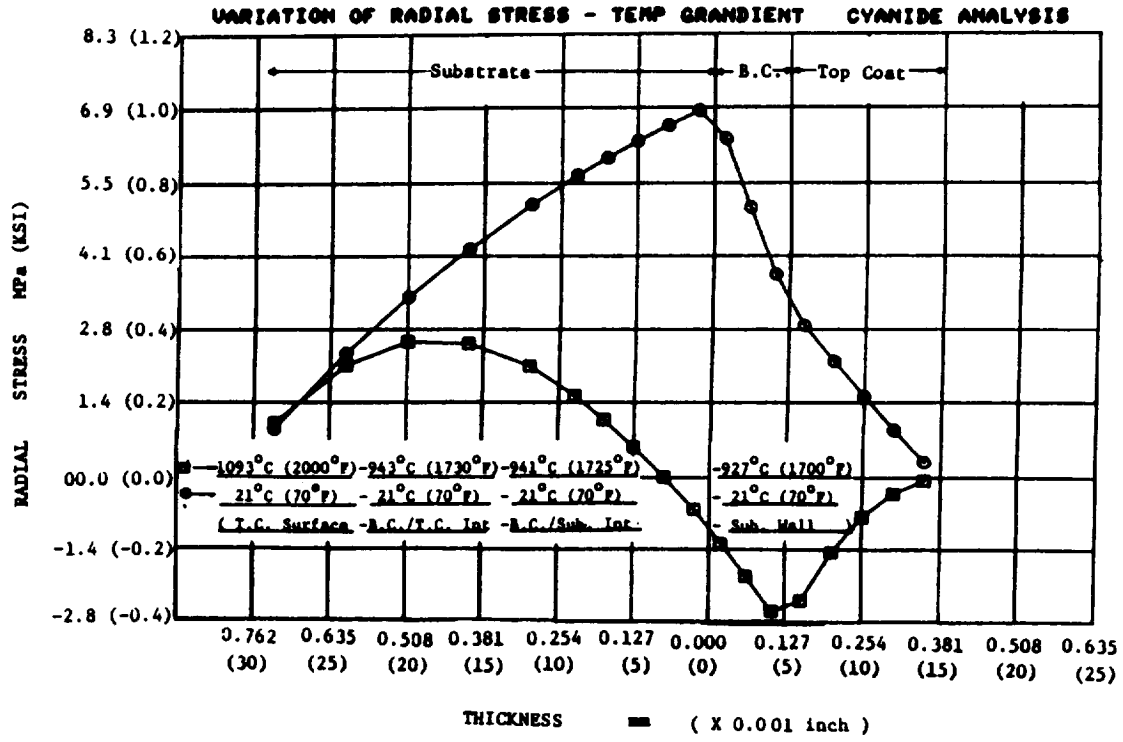

Figure 15b

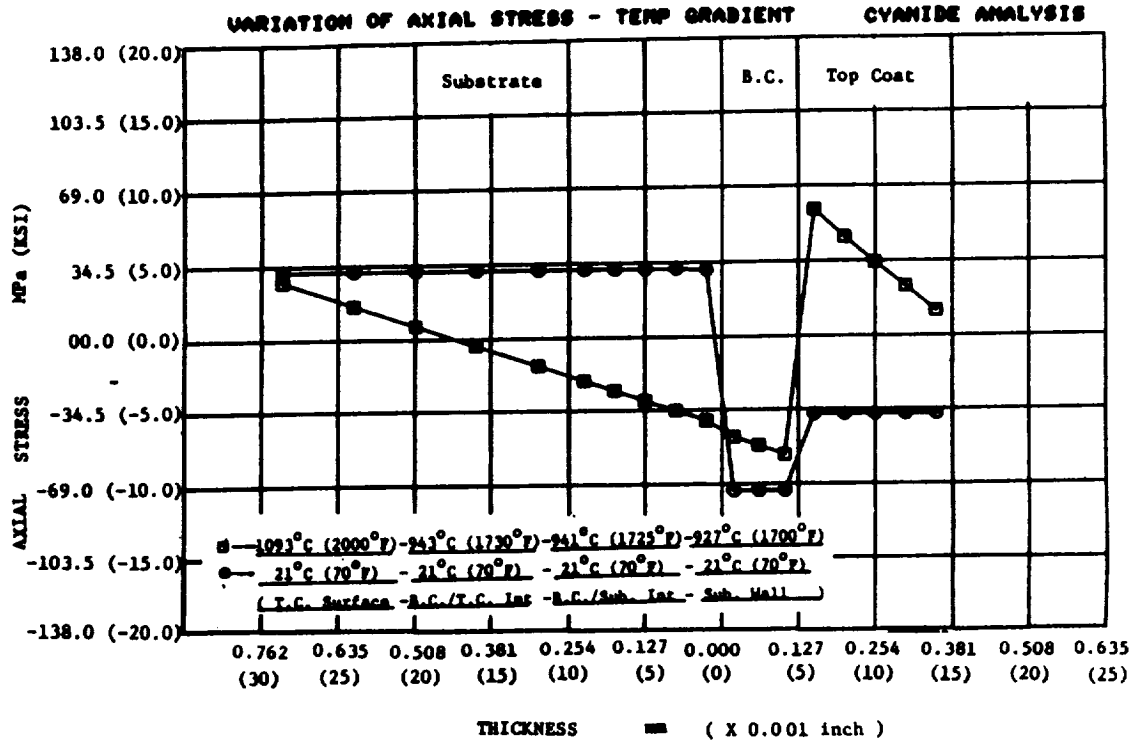

Figure 15c

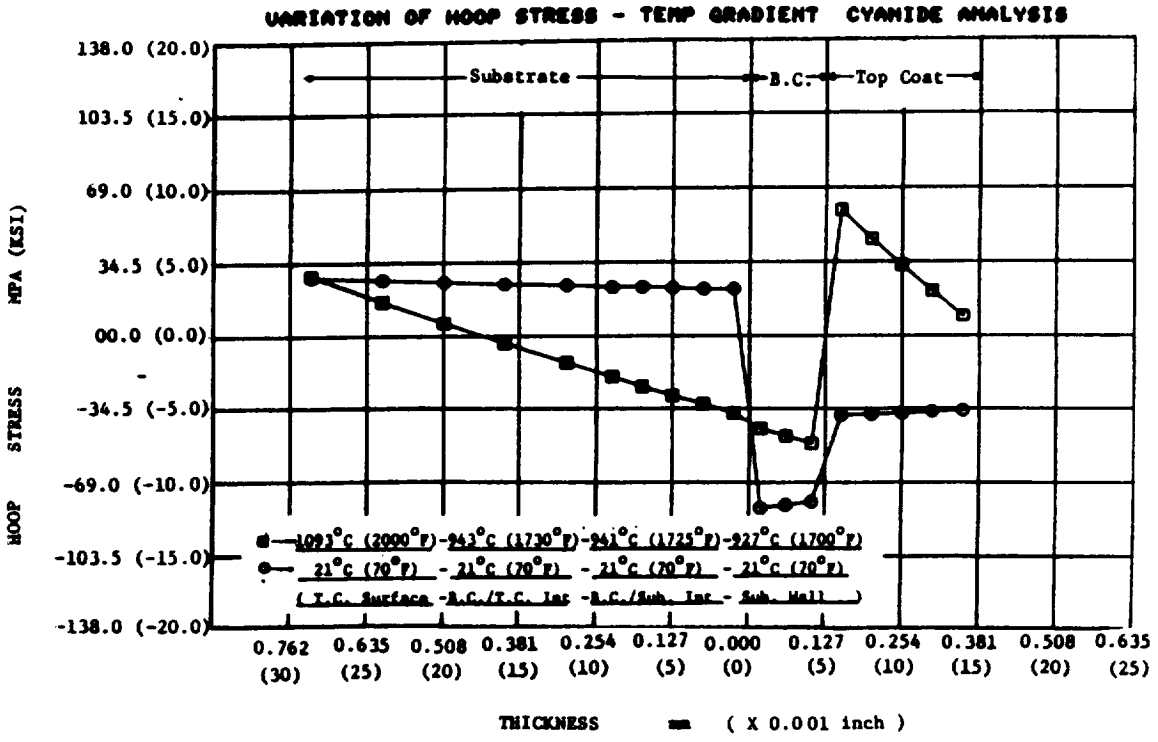

Figure 15d

LCF TUBULAR SPECIMEN

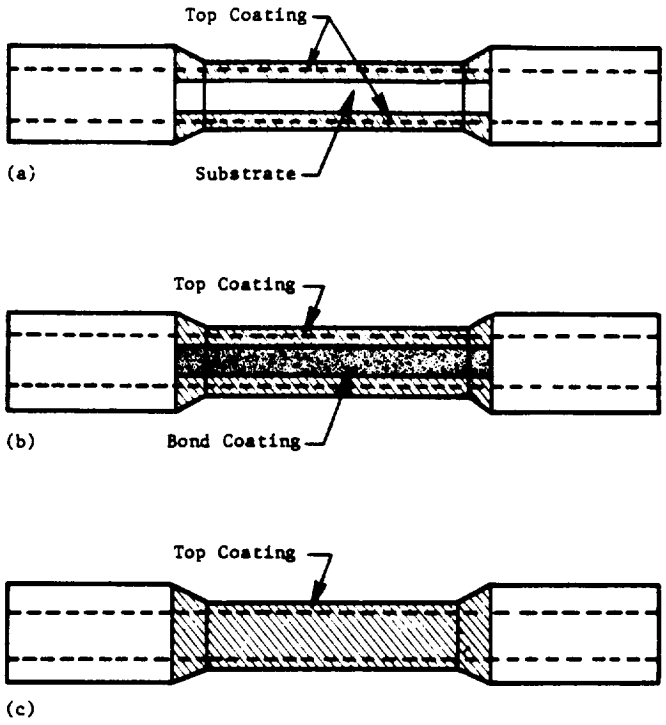

(a) Type 1 - Uncoated Substrate on Gage Section
(b) Type 2 - Uncoated Bond Coat Strip on Gage Section
(c) Type 3 - Fully Coated Gage Section

Figure 16